

Haploinsufficiency of the Sin3/HDAC corepressor complex member *SIN3B* causes a syndromic intellectual disability/autism spectrum disorder

Xenia Latypova,^{1,2,3,27} Marie Vincent,^{1,3,27} Alice Mollé,^{4,27} Oluwadamilare A. Adebambo,^{2,27} Cynthia Fourgeux,⁴ Tahir N. Khan,^{2,5} Alfonso Caro,⁶ Monica Rosello,⁶ Carmen Orellana,⁶ Dmitriy Niyazov,⁷ Damien Lederer,⁸ Marie Deprez,⁹ Yline Capri,¹⁰ Peter Kannu,¹¹ Anne Claude Tabet,¹² Jonathan Levy,¹² Emmelien Aten,¹³ Nicolette den Hollander,¹³ Miranda Splitt,¹⁴ Jagdeep Walia,¹⁵ Ladonna L. Immken,¹⁶ Pawel Stankiewicz,¹⁷ Kirsty McWalter,¹⁸ Sharon Suchy,¹⁸ Raymond J. Louie,¹⁹ Shannon Bell,¹⁹ Roger E. Stevenson,¹⁹ Justine Rousseau,²⁰ Catherine Willem,²¹ Christelle Retiere,^{21,22,23} Xiang-Jiao Yang,²⁴ Philippe M. Campeau,²⁰ Francisco Martinez,⁶ Jill A. Rosenfeld,¹⁷ Cédric Le Caignec,^{1,3} Sébastien Küry,^{1,3} Sandra Mercier,^{1,3} Kamran Moradkhani,¹ Solène Conrad,¹ Thomas Besnard,^{1,3} Benjamin Cogné,^{1,3} Nicholas Katsanis,^{2,25,26} Stéphane Bézieau,^{1,3} Jeremie Poschmann,^{4,28,*} Erica E. Davis,^{25,26,28,*} and Bertrand Isidor^{1,3,28,*}

Summary

Proteins involved in transcriptional regulation harbor a demonstrated enrichment of mutations in neurodevelopmental disorders. The Sin3 (Swi-independent 3)/histone deacetylase (HDAC) complex plays a central role in histone deacetylation and transcriptional repression. Among the two vertebrate paralogs encoding the Sin3 complex, *SIN3A* variants cause syndromic intellectual disability, but the clinical consequences of *SIN3B* haploinsufficiency in humans are uncharacterized. Here, we describe a syndrome hallmarked by intellectual disability, developmental delay, and dysmorphic facial features with variably penetrant autism spectrum disorder, congenital malformations, corpus callosum defects, and impaired growth caused by disruptive *SIN3B* variants. Using chromosomal microarray or exome sequencing, and through international data sharing efforts, we identified nine individuals with heterozygous *SIN3B* deletion or single-nucleotide variants. Five individuals harbor heterozygous deletions encompassing *SIN3B* that reside within a ~230 kb minimal region of overlap on 19p13.11, two individuals have a rare nonsynonymous substitution, and two individuals have a single-nucleotide deletion that results in a frameshift and predicted premature termination codon. To test the relevance of *SIN3B* impairment to measurable aspects of the human phenotype, we disrupted the orthologous zebrafish locus by genome editing and transient suppression. The mutant and morphant larvae display altered craniofacial patterning, commissural axon defects, and reduced body length supportive of an essential role for Sin3 function in growth and patterning of anterior structures. To investigate further the molecular consequences of *SIN3B* variants, we quantified genome-wide enhancer and promoter activity states by using H3K27ac ChIP-seq. We show that, similar to *SIN3A* mutations, *SIN3B* disruption causes hyperacetylation of a subset of enhancers and promoters in peripheral blood mononuclear cells. Together, these data demonstrate that *SIN3B* haploinsufficiency leads to a hitherto unknown intellectual disability/autism syndrome, uncover a crucial role of *SIN3B* in the central nervous system, and define the epigenetic landscape associated with Sin3 complex impairment.

Impairment of transcriptional regulation has been linked closely to the molecular etiology of intellectual disability (ID) and autism spectrum disorders (ASDs).^{1–3} Specifically, multiple genes mutated in Mendelian disorders with a neurodevelopmental or neuroanatomical aspect, and notably ID/ASD genes, have been found to encode

¹Service de Génétique Médicale, CHU Nantes, 9 quai Moncousu, 44093 Nantes Cedex 1, France; ²Center for Human Disease Modeling, Duke University Medical Center, Durham, NC 27701, USA; ³L'Institut du Thorax, INSERM, CNRS, Université de Nantes, 44007 Nantes, France; ⁴Université de Nantes, CHU Nantes, Inserm, Centre de Recherche en Transplantation et Immunologie, UMR 1064, ITUN, 44000 Nantes, France; ⁵Department of Biological Sciences, National University of Medical Sciences, 46000 Rawalpindi, Pakistan; ⁶Unidad de Genética, Grupo de Investigación Traslacional en Genética, Hospital Universitario y Politécnico La Fe, 46026 Valencia, Spain; ⁷Department of Pediatrics, Ochsner Clinic, New Orleans, LA 70128, USA; ⁸Centre de Génétique Humaine, IPG, 6041 Gosselies, Belgium; ⁹Service de Neuropédiatrie, Clinique Saint Elizabeth, 5000 Namur, Belgium; ¹⁰Service de Génétique Médicale, Hôpital Robert Debré, 75019 Paris, France; ¹¹Division of Clinical and Metabolic Genetics, The Hospital for Sick Children, Toronto, ON M5G 1X8, Canada; ¹²Service de Cytogénétique, Hôpital Robert Debré, 75019 Paris, France; ¹³Department of Clinical Genetics, Leiden University Medical Center, 2333 Leiden, the Netherlands; ¹⁴Northern Genetics Service, Institute of Genetic Medicine, Newcastle Upon Tyne NE1 3BZ, UK; ¹⁵Kingston General Hospital Research Institute, 76 Stuart Street, Kingston, ON K7L 2V7, Canada; ¹⁶Clinical Genetics, Dell Children's Medical Group, Austin, TX 78731, USA; ¹⁷Department of Molecular and Human Genetics, Baylor College of Medicine, Houston, TX 77030, USA; ¹⁸GeneDx, 207 Perry Parkway, Gaithersburg, MD 20877, USA; ¹⁹Greenwood Genetic Center, 106 Gregor Mendel Cir, Greenwood, SC 29646, USA; ²⁰Sainte-Justine Hospital, 3175, Cote-Sainte-Catherine, Montreal, QC, Canada; ²¹Etablissement Français du Sang, 44000 Nantes, France; ²²CRCINA, INSERM, CNRS, Université d'Angers, Université de Nantes, 44000 Nantes, France; ²³LabEx IGO, Nantes 44000, France; ²⁴Rosalind & Morris Goodman Cancer Research Center and Department of Medicine, McGill University, Montreal, QC H3A 1A3, Canada; ²⁵Advanced Center for Translational and Genetic Medicine, Stanley Manne Children's Research Institute, Ann & Robert H. Lurie Children's Hospital of Chicago, Chicago, IL 60611, USA; ²⁶Department of Pediatrics, Feinberg School of Medicine, Northwestern University, Chicago, IL 60611, USA

²⁷These authors contributed equally

²⁸These authors contributed equally

*Correspondence: bertrand.isidor@chu-nantes.fr (B.I.), eridavis@luriechildrens.org (E.E.D.), jeremie.poschmann@univ-nantes.fr (J.P.)

<https://doi.org/10.1016/j.ajhg.2021.03.017>

© 2021 American Society of Human Genetics.



chromatin regulators.^{4–6} Eukaryotic chromatin structure is organized in histone octamers of the four core histones, H2A, H2B, H3, and H4, forming nucleosomes to ensure DNA compaction. Post-translational modifications of histone N termini, particularly acetylation, play decisive roles in the dynamic regulation of gene transcription. Histone deacetylation is executed by the histone deacetylase (HDAC) enzymes HDAC1 and HDAC2 and is dependent upon complexes containing Sin3, MecP2,⁷ NuRD, and CoREST.^{8–10} Recruitment of the Sin3 corepressor module leads to deacetylation of histones H3 and H4.¹¹ The core SIN3-HDAC complex acts as a scaffold for the assembly of multiple cofactors.^{12–14} In mammals, two genes encode master factors of the Sin3 complex, *SIN3A* (MIM: 607776) and *SIN3B* (MIM: 607777). *SIN3A* disruption in humans causes syndromic ID with craniofacial defects (Witteveen-Kolk syndrome [MIM: 613406]).¹⁵ Consequences of *SIN3B* disruption in humans are hitherto poorly understood.

In this study, we report the phenotypic features associated with haploinsufficiency at the *SIN3B* locus through combined analysis of clinical and cerebral MRI data collected for nine individuals harboring rare *SIN3B* variants (seven *de novo* and two of undetermined origin due to an inaccessible parental sample). We identified five copy number variant (CNV) deletions at 19q13.11, which encompass *SIN3B* (0.427 to 1.5 Mb; smallest region of overlap, SRO, ~230 kb, hg19), and four single nucleotide variants (SNV) in the coding regions of *SIN3B* (Table 1). To investigate the consequences of *SIN3B* loss *in vivo*, we ablated *sin3b* in zebrafish (*Danio rerio*) larvae with a transgenic reporter of cartilage formation in the pharyngeal skeleton by CRISPR/Cas9 genome editing and transient morpholino (MO)-based suppression. We recapitulate multiple aspects of the human phenotype in zebrafish and demonstrate pathogenicity for the two missense variants. Furthermore, we investigated the epigenetic consequences of *SIN3B* variation by epigenomic profiling the peripheral blood mononuclear cells (PBMCs) from an affected CNV deletion-bearing individual compared with his family members and compared with data generated from PBMCs from a *SIN3A* CNV deletion pedigree. The results suggest that *SIN3B* disruption leads to increased histone acetylation in this individual, which is consistent with *SIN3A* ablation and the repressor function of the Sin3 complex.

Nine affected individuals were referred independently for genetic counseling and clinical genetic testing because of unexplained ID or ASD (Table 1). We obtained written informed consent from each affected individual and available family members prior to inclusion in genetics research in accordance with each respective institution's human subjects ethics committee. All participants were assessed by at least one expert clinical geneticist from each respective participating center (Table 1; supplemental notes).

To investigate the possibility that CNVs could contribute to the ID/ASD features, we performed chromosomal micro-

array studies (Table S1). Individuals 1, 2, 3, 4, and 5 carry microdeletions of 1.02, 1.5, 0.87, 0.88, and 0.43 Mb, respectively, at the 19p13.11 locus, all of which encompass *SIN3B* (Figure 1A; Table S2). Notably, *de novo* deletions of this chromosomal region have been implicated previously in multi-system pathologies in humans, including neurodevelopmental disorders. Aten and colleagues reported an affected male who harbored a 0.99 Mb *de novo* deletion that contains 28 genes (Table 1; Table S2),¹⁶ and Bens et al. described a female pediatric affected individual with an overlapping 1.12 Mb microdeletion at 19p13.11 (Table 1; Table S2).¹⁷ Comparison of the microdeletions reported in these two affected individuals with the five individuals in our study yielded a smallest region of overlap (SRO) of ~230 kb, which contains four genes (*NWD1* [MIM: 616250], *SIN3B*, *F2RL3* [MIM: 602779], and *CPAMD8* [MIM: 608841]; Figure 1A; Table S2). *In silico* predictions suggested *SIN3B* to be the most likely candidate disease driver gene because of its high probability of loss of function (LoF) intolerance (pLI) score¹⁸ (*SIN3B* pLI > 0.9; *NWD1*, *F2RL3*, *CPAMD8* pLI = 0; Table S2). Individual 3 carried an additional *de novo* deletion of 1.6 Mb at 18p11.31 (chr18: 3,192,682–4,854,252, GRCh37/hg19), encompassing four genes (*MYOM1* [MIM: 603508], *MYL12B* [MIM: 609211], *TGIF1* [MIM: 602630], and *DLGAP1* [MIM: 605445]). *TGIF1* loss-of-function variants have been described in holoprosencephaly type 4 (MIM: 142946).¹⁹ *MYOM1*, *MYL12B*, and *DLGAP1* have not been linked to a human disorder. However, this second mutational event most likely plays a role in the phenotype of individual 3. Additionally, the individual described by Aten et al. presents with split hand and foot malformation (SHFM) (Table 1).¹⁶ *EPS15L1* (MIM: 616826) was considered to be responsible for the limb phenotype and is not included in the SRO reported in our study (Figure 1; Table S2).

Next, we asked whether pathogenic variants in any of these genes in the SRO had been implicated in phenotypes overlapping with 19p13.11 deletion carriers. *NWD1* and *F2RL3* have not been implicated previously in human genetic disorders. Bi-allelic mutations in *CPAMD8* cause anterior segment dysgenesis²⁰ (MIM: 617319), but carriers of heterozygous loss-of-function variants are not known to have neurodevelopmental symptoms. Individual 3 presents with ocular anterior segment dysgenesis (Table 1), and we cannot exclude the possibility of a variant in *CPAMD8* on the non-deleted allele that could explain a part of this individual's ocular phenotype. However, a likely disruptive variant was identified in *SIN3B* in a previous study within a large syndromic ID cohort²¹ but was only reported as a candidate because of a lack of genetic evidence in support of causality. Here, we report the same individual with the frameshift *de novo* variant located in exon 1 of *SIN3B* (c.31delA [p.Ser11Alafs*11] [GenBank: NM_015260.4]) as individual 6 (Figure 1B; Table 1). This SNV is absent from >240,000 alleles in the Genome Aggregation Database (gnomAD; accessed September 22, 2019),

Table 1. Clinical features of five individuals with *de novo* 19p13.11 microdeletions encompassing *SIN3B* and four individuals with point mutations in *SIN3B*

Individual identifier	1	2	3	4	5	6	7	8	9	Total	Aten et al., 2009 ¹⁶	Bens et al., 2011 ¹⁷
DECIPHER identifier (v.9.21)	332280	262142	NA	NA	308455	325602	NA	NA	NA	NA	4101	NA
Genotype^{a,b}												
Variant type	CNV, deletion	CNV, deletion	CNV, deletion	CNV, deletion	CNV, deletion	SNV, frameshift	SNV, frameshift	SNV, nonsynonymous	SNV, nonsynonymous	5 CNV del, 4 SNV	CNV, deletion	CNV, deletion
Inheritance	<i>de novo</i>	<i>de novo</i>	<i>de novo</i>	<i>de novo</i>	<i>de novo</i>	<i>de novo</i>	parents unavailable for testing	<i>de novo</i>	father unavailable for testing	7 confirmed <i>de novo</i>	<i>de novo</i>	<i>de novo</i>
Variant details	19: 16848440–17871985	19: 15978604–17500427	19: 16599950–17469382	19: 16456955–17333482	19: 16652215–17079033	c.31delA (p.Ser11Alafs*11)	c.1579delC (p.Arg527Glyfs*12)	c.249C>G (p.Ile83Met)	c.58G>A (p.Gly20Arg)	NA	19: 16548375–17547292	19: 16611808–17733344
Size	1.02 Mb	1.52 Mb	869 kb	877 kb	427 kb	NA	NA	NA	NA	NA	0.99 Mb	1.12 Mb
Clinical phenotypes												
Sex	M	F	M	F	M	M	M	M	M	NA	M	F
Age at last clinical examination	20 years	11 years	2 years 6 months	8 years 10 months	3 years 10 months	15 years	50 years 4 months	3 years	5 years	NA	6 years	4 years
Growth parameters	W: -4 SD, H: -2 SD, OFC: 0 SD	W: +1 SD, H: -0.5 SD, OFC: -0.5 SD	W: -0.5 SD, H: N, OFC: -3 SD	W: -1 SD, H: +0.5 SD, OFC: -1.5 SD	W: -0.75 SD, H: -1.04 SD, OFC: -0.97 SD	W: +3 SD, H: +2.5 SD, OFC: +2.5 SD	W: -1 SD, H: -2 SD, OFC: N	W: +1.2 SD, H: -0.5 SD, OFC: -0.5 SD	W: +2 SD, H: +2 SD, OFC: +2 SD	NA	W: ND, H: -0.3 SD, OFC: -1 SD	W: -1.4 SD, H: -1.9 SD, OFC: -3.5 SD
DD/ID	- (IQ 96)	+ (IQ 41)	+ (IQ ND)	+ (WISC-IV)	+ (IQ ND)	+ (IQ ND)	+ (IQ 56)	+ (IQ ND)	+ (IQ ND)	8/9	+ (IQ ND)	+ (IQ ND)
DD/ID severity	NA	moderate	moderate	mild	mild	mild	mild	moderate	mild	5 mild, 3 moderate	severe	severe
Age at independent walking	18 months	2 years 8 months	2 years 4 months	13 months	24 months	24 months	ND	22 months	18 months	NA	ND	ND
Speech delay	-	+	+	- (articulation problems)	-	+	+	+	+	6/9	+	+
ASD	+	-	-	-	-	+	-	-	+	3/9	-	-
Other behavioral disorders	ADHD	ADHD	-	hyperactivity, impulsivity, low frustration tolerance, anxiety	-	aggressive behavior	echolalia	-	ADHD	6/9	-	-

(Continued on next page)

Table 1. Continued

Individual identifier	1	2	3	4	5	6	7	8	9	Total	Aten et al., 2009¹⁶	Bens et al., 2011¹⁷
Epilepsy	–	–	–	–	–	–	+	–	–	1/9	–	–
Brain MRI	N	N	short CC, olfactory bulb agenesis	mild tonsillar ectopia	ND	defects in CC and subependymal nodular heterotopia	N	ND	ND	3/6	ND	ND
Dysmorphic features^c	+	+	+	+	+	+	+	+	+	9/9	+	+
Limb abnormalities	short hands	bilateral fifth fingers clinodactyly, genu recurvatum	–	clinodactyly of the 2 nd and 5 th digits, tapered distal phalanges	–	–	–	–	bilateral radio-ulnar synostosis	4/9	SHFM	–
MCA	–	VSD, bifid uvula, strabismus	VSD, left iris coloboma, ocular anterior segment dysgenesis, left cleft lip and palate, micropenis	bifid uvula, strabismus	tetralogy of Fallot, preauricular pit	–	–	intestinal malrotation	ND	5/8	tetralogy of Fallot	–
Additional phenotypic features	myopia, daytime hypersomnia, decreased melatonin urinary excretion	ataxia	–	umbilical hernia, clumsiness, myopia, hypotonia	pectus carinatum	conductive hearing loss	hand tremor	–	ND	NA	strabismus	initial poor feeding, premature pubarche, strabismus, ataxia
Additional genetic findings	–	–	CNV deletion (1.6 Mb) <i>de novo</i> , 18:3192682–4854252	–	–	–	–	–	<i>CNOT1</i> c.4861A>G (p.Ile1621Val) (unknown inheritance)	NA	ND	ND

Abbreviations are as follows: NA, not applicable; M, male; F, female; W, weight; H, height; OFC, occipitofrontal head circumference; SD, standard deviation; ND, no data; N, normal; DD, developmental delay; ID, intellectual disability; WISC-IV, Wechsler Intelligence Scale for Children; ASD, autism spectrum disorder; MRI, magnetic resonance imaging; MCA, multiple congenital anomalies; ADHD, attention deficit hyperactivity disorder; CC, corpus callosum; VSD, ventricular septal defect; SHFM, split hand and foot malformation; p, percentile; +, affected; –, not affected; CNV, copy number variant; del, deletion; SNV, single-nucleotide variant.

^aThe reference genome used for annotations is GRCh37/hg19.

^bCoding DNA/protein variant described according to the nomenclature HGVS v.2.0 established by the Human Genome Variation Society; GenBank: NM_015260.4 and NP_056075.1.

^cFor dysmorphic features, see [supplemental notes](#).

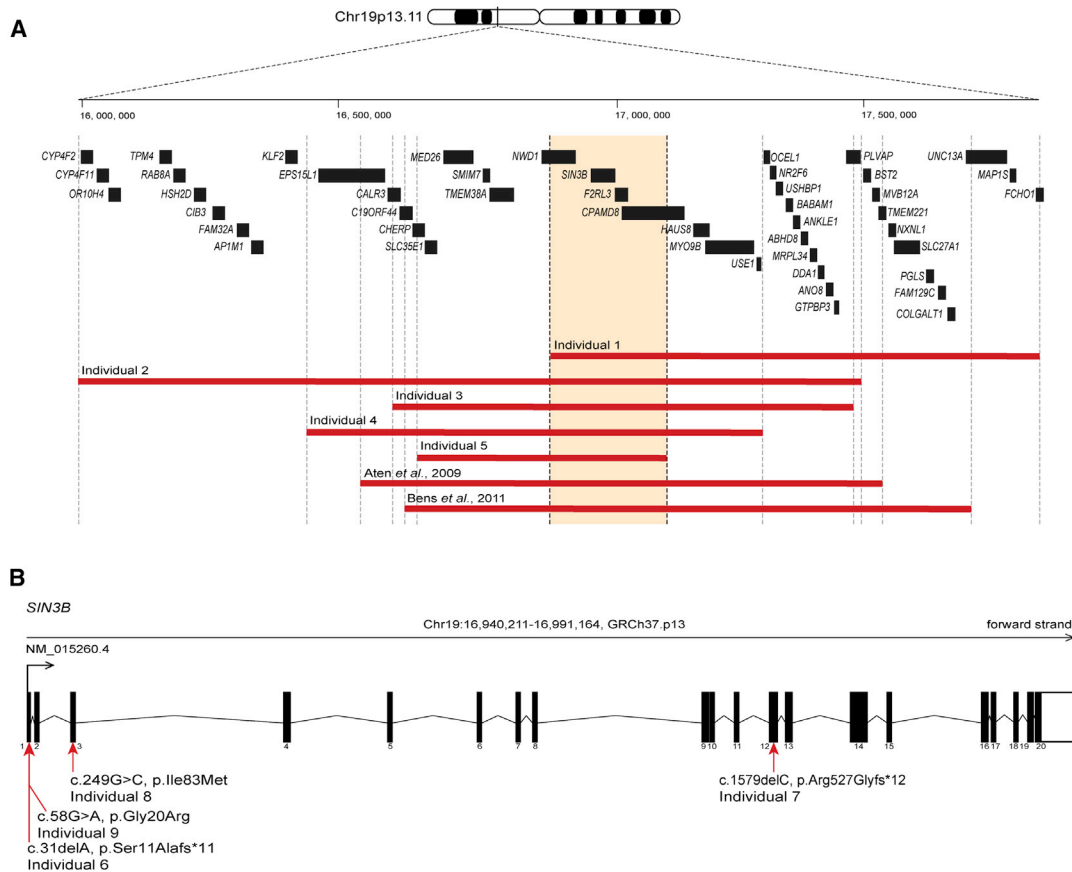


Figure 1. Copy number variants and single nucleotide variants altering *SIN3B* cause intellectual disability with autistic features
 (A) Schematic depicting *SIN3B* (GRCh37.p13; chr19: 16,940,211–16,991,164) at the 19p13.11 locus. CNV deletions (red bars) encompassing *SIN3B* in individuals 1, 2, 3, 4, and 5, as well as two previously reported individuals,^{16,17} are shown. Gene positions are indicated by black boxes, and genes located in smallest region of overlap are included in orange box between vertical dashed lines.
 (B) Exon structure of longest *SIN3B* transcript, containing 20 exons (GenBank: NM_015260.4). Variants c.31delA (p.Ser11Alafs*11) (individual 6); c.1579delC (p.Arg527Glyfs*12) (individual 7); c.249C>G (p.Ile83Met) (individual 8); and c.58G>A (p.Gly20Arg) (individual 9) are indicated with red arrows.

and the variant transcript is predicted to be degraded by nonsense-mediated decay, resulting in *SIN3B* haploinsufficiency. However, cell lines derived from the affected individual were not available to test this possibility experimentally.

We turned to community data-sharing platforms²² to ask whether additional affected individuals might be present with deleterious mutations and overlapping clinical features at this locus. We identified individual 7, who carries a c.1579delC (p.Arg527Glyfs*12) frameshift variant in exon 12 (Figure 1B; Table 1). Parental samples were not available for segregation analysis. Exome sequencing (ES) of individual 8 identified a *de novo* c.249C>G (p.Ile83Met) change that is predicted to be damaging by *in silico* classifiers and is absent from gnomAD (Figures 1B, 2, and S1; Tables 1, S1, and S3). This change affects a conserved residue within the first paired amphipathic helix (PAH) domain of *SIN3B*, which is responsible for interaction with members of Sin3/HDAC complex (Figures 2 and S1). Individual 9 harbors a heterozygous c.58G>A (p.Gly20Arg) variant (Figures 1B, 2, and S1; Tables 1 and S1). This variant is absent from gnomAD and is predicted to be deleterious *in silico* (Table

S3). This change was not detected in genomic DNA from individual 9's mother, but the paternal sample was not available to confirm the mode of inheritance. Individual 9 also harbors a variant of uncertain significance in *CNOT1* (MIM: 604917), a locus known to cause either dominant holoprosencephaly^{23,24} (MIM: 618500) or Vissers-Bodmer syndrome²⁵ (MIM:619033; c.4861A>G [p.Ile1621Val] [GenBank: NM_001265612.2]), for which contribution to the phenotype cannot be excluded (Table 1). Even so, we considered this *SIN3B* variant, in combination with individual 9's neurodevelopmental phenotypes, to be potentially relevant to our case series. Together, these two ultra-rare missense variants were supportive, but not conclusive, in implicating *SIN3B* involvement in the ID/developmental delay (DD) phenotypes observed in individuals 1–5, who harbor CNVs on 19p13.11, and in individuals 6 and 7, who harbor frameshift variants.

All nine individuals presented with a constellation of cognitive and neuroanatomical phenotypes. The most frequently reported features included ID and DD (in 8/9), classified as mild (individuals 4, 5, 6, 7, and 9) and moderate (individuals 2, 3, and 8; Table 1). In addition to ID/DD,

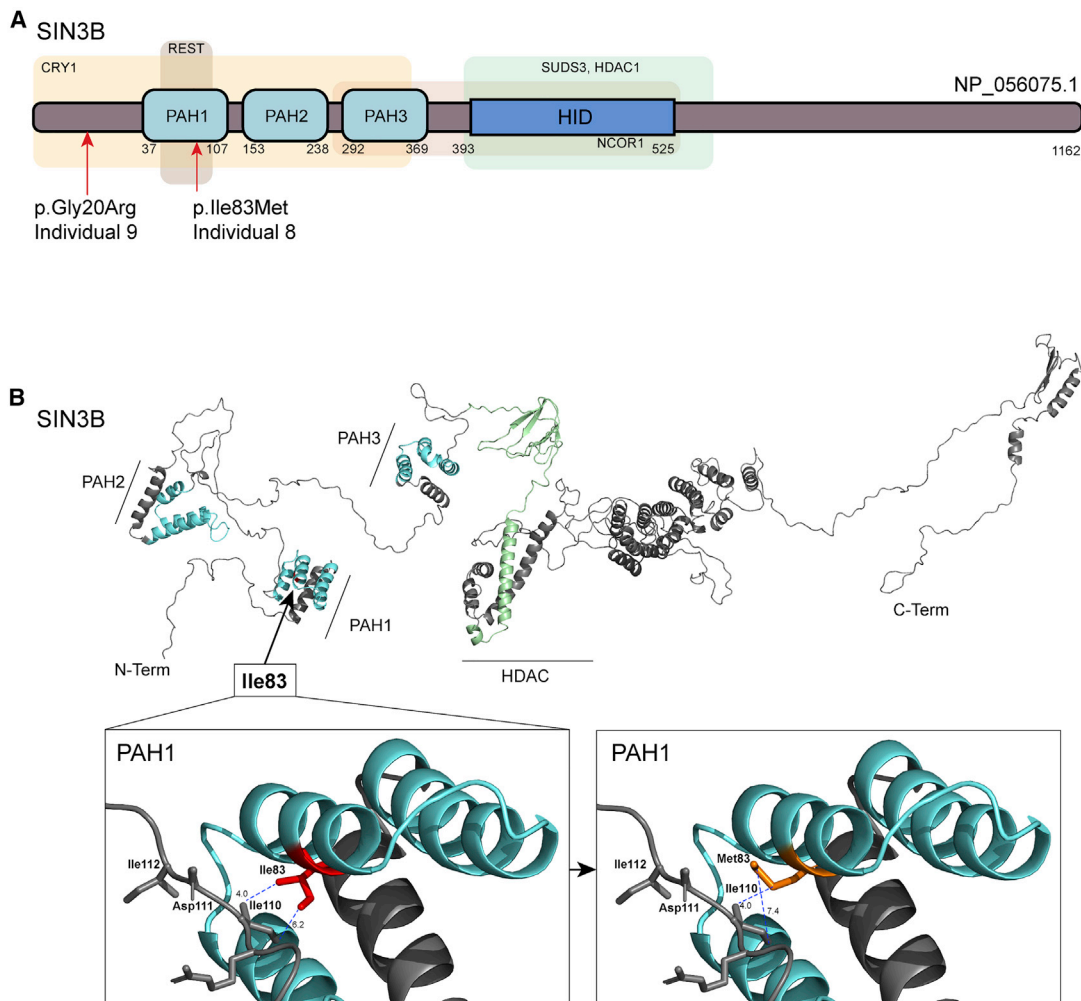


Figure 2. *In silico* protein modeling of *SIN3B* nonsynonymous variants indicate likely disruption of protein function

(A) *SIN3B* protein structure (GenBank: NP_056075.1). Three paired amphipathic helix (PAH domains) predicted on the N-terminal region of *SIN3B* are indicated by light blue boxes. Regions that interact (predicted by similarity with murine *Sin3b*) with *CRY1* (cryptochrome circadian clock 1), *REST* (RE1-silencing transcription factor), *SUDS* (*Sin3* histone deacetylase corepressor complex component *SDS*), *HDAC1* (histone deacetylase 1), *NCOR1* (nuclear receptor corepressor 1), and *HID* (HDAC-interacting domain) are indicated by light-colored boxes.

(B) *In silico* three-dimensional view of *SIN3B*. Variant c.249C>G encodes p.Ile83Met, which affects a residue located in the PAH1 domain nearest to the N terminus, which is predicted to mediate protein-protein interaction with transcriptional corepressors *REST* and *CRY1*. Protein Data Bank (PDB) file was generated by RaptorX and analyzed in Pymol 2.0. PAH domains are colored in turquoise and *HID* is colored in light green. Distance (Å) between side chains of wild-type (Ile83; left box) and mutant (Met83; right box) *SIN3B* and the closest residue on the opposing side of the protein are measured as indicated (blue dashed lines).

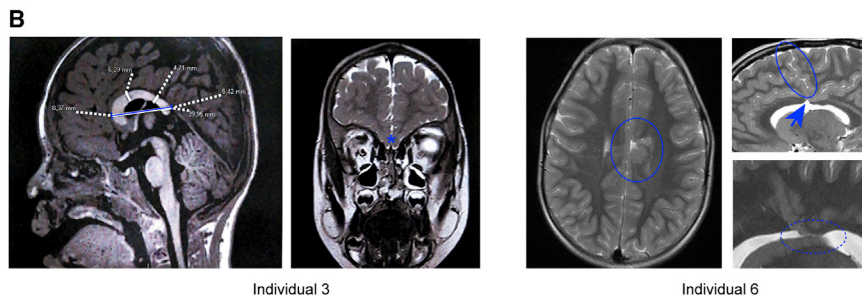
three individuals fulfilled clinical diagnostic criteria for ASD (individuals 1, 6, and 9). Moreover, three individuals had attention deficit hyperactivity disorder (ADHD; individuals 1, 2, and 9). Cerebral MRI showed variable features; these included corpus callosum defects and subependymal nodular heterotopia (individual 6, Figure 3B), hypoplastic corpus callosum (individual 3, who also has a *TGIF1* deletion), and mild tonsillar ectopia (individual 4); the other half of the cohort presented no detectable MRI abnormalities at last assessment or did not have brain imaging (Table 1). Individual 7 had generalized tonic-clonic seizures starting at age 3. Some individuals presented with short stature for age (individuals 1 and 7). Additionally, cardiac defects were present in three individuals, specifically ventricular

septal defect (VSD; individuals 2 and 3) and tetralogy of Fallot (individual 5). Three individuals presented with labiopalatine cleft or bifid uvula (individuals 2, 3, and 4). Although several affected individuals displayed dysmorphic facial features, including broad nasal root, arched and full eyebrows, synophrys, or epicanthus, no unifying facial gestalt was evident across all affected individuals (Figure 3A).

Zebrafish mutants harboring truncating mutations in *sin3b* display locomotion defects, delayed ossification, and shortened body length.²⁶ With the exception of variable growth phenotypes in our cohort (Table 1), these aberrant zebrafish mutant phenotypes did not have discrete anatomical correlates with features of our human cohort.



Individual 3 Individual 7 Individual 8



Individual 3 Individual 6

Figure 3. Facial photographs and magnetic resonance imaging (MRI) of individuals who harbor CNVs or SNVs impacting *SIN3B*

(A) Front view of individual 3, who has an 869 kb deletion CNV; note the bulbous nose, arched eyebrows, epicanthus, broad nasal root, and prominent forehead. Front view of individual 7, who harbors the c.1579delC (p.Arg527Glyfs*12) variant; note large ears and full and arched eyebrows. Front view of individual 8, carrying the c.249C>G (p.Ile83Met) variant; note prominent coronal suture, arched eyebrows, and small palpebral fissures.

(B) Brain MRI from individuals 3 and 6. Individual 3: note short corpus callosum (blue segment) and olfactory bulb agenesis (asterisk). Individual 6: note polymicrogyria (blue circle) with corpus callosum defects (blue arrow) and subependymal nodular heterotopia (dotted blue circle).

To test whether we could link anatomical phenotypes observed in individuals with *SIN3B* haploinsufficiency, we disrupted the *SIN3B* ortholog in zebrafish (Ensembl: ENSDARG0000062472, GRCz10; 63% identity, 74% similarity versus human [GenBank: NP_056075.1]; Figure S2A). All experiments involving zebrafish were approved by the Duke University Institutional Animal Care and Use Committee. These experiments were performed at least twice with similar results, with the investigator masked to experimental condition, and all statistical comparisons were performed with a non-parametric Kruskal-Wallis test. We generated F0 mutant models by targeting exon 13 of *sin3b* by using CRISPR/Cas9 genome editing; we confirmed a high level of mosaicism for frameshifting events through heteroduplex analysis and sequencing of PCR amplicons flanking the target sites (>90%; Figures S2A and S2B).

Given that several individuals in our study displayed dysmorphic facial features (Figure 3A), we first focused on cartilage patterning as a readout for *sin3b* effects on development. We and others have shown previously that morphometric assessment of the pharyngeal skeleton in zebrafish is directly relevant to craniofacial features associated with neurodevelopmental defects in humans.^{27–33} We injected guide RNA (gRNA) and Cas9 protein into the cell of single cell-staged embryos carrying a *1.4col1a1:egfp* transgene,³⁴ performed live bright-field and fluorescent imaging at 3 days post fertilization (dpf), and analyzed cartilaginous ventral structures of the developing larval head by measuring the ceratohyal (CH) angle. *sin3b* F0 mutants display a significantly increased CH angle compared with control larvae or larvae injected with gRNA alone, supporting a role for the Sin3 complex in patterning of anterior facial structures ($p < 0.0001$, gRNA + Cas9 versus gRNA alone or controls; $n = 21–34$ larvae/batch; repeated, masked scoring; Figures 4A–4C). Additionally, and consistent with stable *sin3b* mutants,²⁶ *sin3b* F0 larvae display significantly shorter body length compared with control

larvae or larvae injected with gRNA alone ($p < 0.0001$, gRNA + Cas9 versus gRNA alone; $p < 0.005$, gRNA + Cas9 versus controls; $n = 21–27$ larvae/batch; repeated, masked scoring; Figure 4C). Further, to detect neuroanatomical defects, we investigated the integrity of commissural axon tracts in the zebrafish brain at 3 dpf as a proxy for the corpus callosum defects observed in two affected individuals with *SIN3B* variants. We fixed larvae, immunostained with acetylated tubulin antibody, and quantified the number of intertectal neurons crossing the dorsal midline between the optic tecta as described.³⁵ We observed a significant depletion of commissural axons in *sin3b* F0 mutants compared with both gRNA alone batches or uninjected controls (Figures 4D and 4E; $p < 0.0001$ for gRNA + Cas9 versus gRNA alone or controls; $n = 49–50$ larvae/batch; repeated).

We then confirmed the specificity of the craniofacial and body length phenotypes in F0 mutants by performing MO-based knockdown of *sin3b*. We obtained a splice-blocking (sb) MO targeting the splice donor site of *sin3b* exon 2 (e2i2), injected it into embryo batches at the one-to-four cell stage, and generated cDNA from whole larvae at 3 dpf to monitor mRNA splicing. We performed RT-PCR to amplify and sequence regions of interest encompassing exon 2 and confirmed a frameshifting event induced by exclusion of *sin3b* exon 2 (Figures S3A–S3C). Next, we injected increasing concentrations of e2i2 sb MO (3, 6, and 9 ng) into *-1.4col1a1:egfp* embryos and subjected larvae to the same craniofacial phenotyping paradigm described for F0 mutants. We observed a dose-dependent increase in CH angle in *sin3b* morphants ($p < 0.0001$; $n = 35–58$ larvae/condition; Figure S3D). Moreover, coinjection of e2i2 sb MO with wild-type (WT) human *SIN3B* mRNA (GenBank: NM_015260.4; generated with a commercially obtained ORF clone; Genecopoeia, Z4616) as described³⁶ rescued these craniofacial defects, indicating MO specificity ($p < 0.0001$ for MO versus MO+WT mRNA; $n = 34–72$ larvae/batch; repeated; Figure S3E). To test the

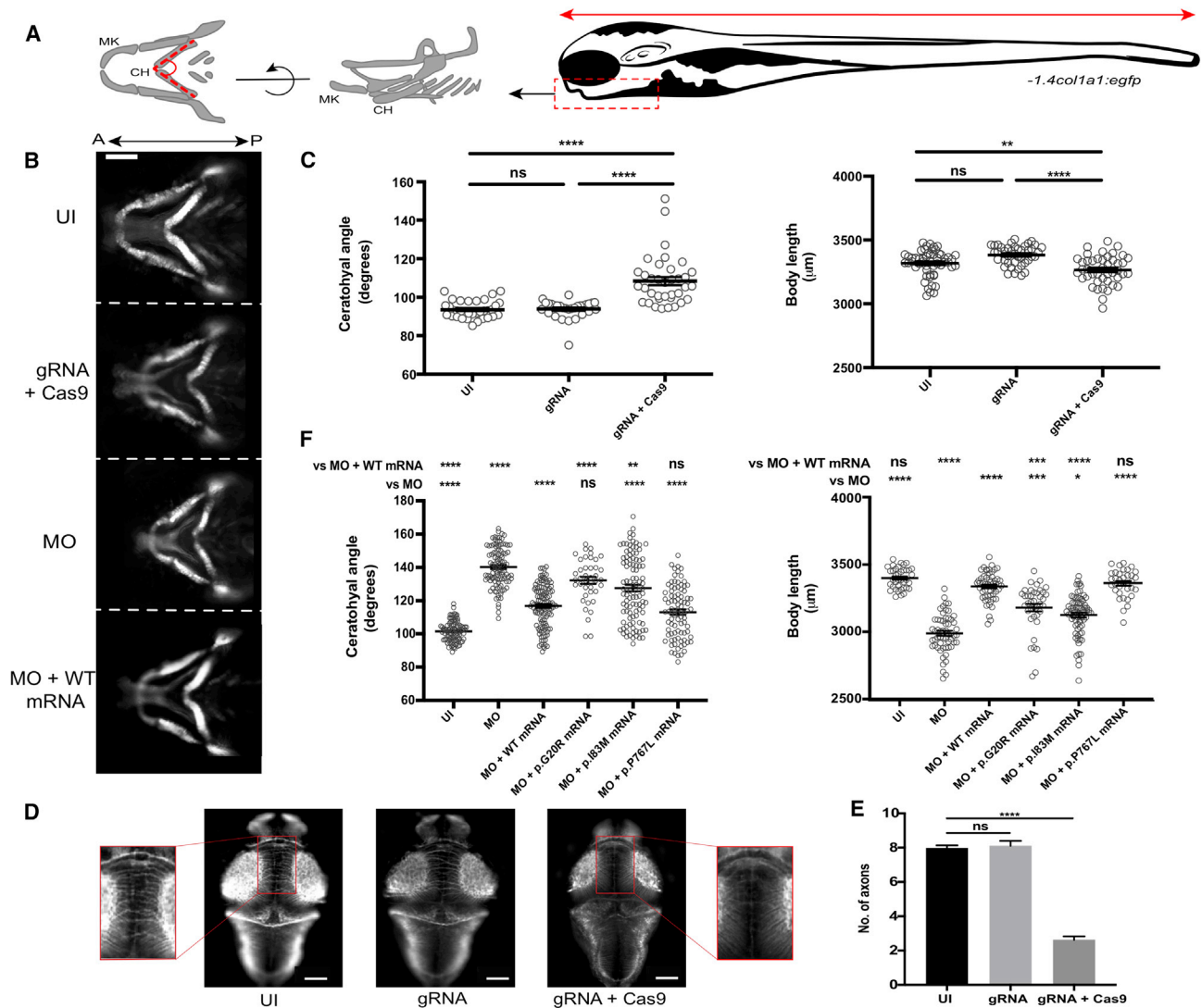


Figure 4. Modeling of *sin3b* disruption in zebrafish shows abnormal craniofacial patterning, reduced body length, and pathogenicity of case-associated missense variants

(A) Schematic of structures of interest used for *in vivo* measurements in developing zebrafish larvae at 3 days post fertilization (dpf); cartilaginous craniofacial structures (left, angle between dashed lines); body length (right, red horizontal arrow); CH, ceratohyal cartilage; MK, Meckel cartilage. *-1.4col1a1:egfp* transgenic zebrafish larvae were positioned with the Vertebrate Automated Screening Technology (VAST) BioImager and ventral fluorescent images were captured as indicated (right panel, red vertical arrow).

(B) Representative ventral images of *in vivo* models of *sin3b* disruption in zebrafish. CH angle was measured as indicated in (A). UI, uninjected; MO, morpholino; WT, human *SIN3B* mRNA. Scale bar, 100 μ m.

(C) Quantification of craniofacial defects and body length in CRISPR/Cas9 F0 mutants. Small insertions and deletions were introduced into *sin3b* exon 13 via a high-efficiency guide RNA (gRNA). Targeting with gRNA leads to an increase of CH angle (left) and decrease in body length (right), indicating a crucial role for the Sin3 complex in the patterning of anterior structures and growth ($n = 21-34$ and $21-27$ larvae/batch, repeated, for craniofacial and body length, respectively).

(D) Representative images showing fluorescent signal detected from the dorsal aspect of fixed and acetylated tubulin antibody-stained 3dpf larvae. Zoomed insets (left and right) show the region assessed for commissural neurons that cross the midline.

(E) Quantification of intertectal neurons in *sin3b* F0 mutants as a proxy for corpus callosum defects in *SIN3B* mutation-bearing humans. $n = 49-50$ larvae/batch, repeated.

(F) Transient suppression models mimic *sin3b* CRISPR F0 mutants. *sin3b* morphants (injected with 9 ng of e2i2 splice-blocking [sb] MO) display a broadened CH angle (left) and shortened body length (right) compared with uninjected controls. Coinjection of *sin3b* e2i2 splice-blocking MO with 100 pg of *SIN3B* WT human mRNA rescues this phenotype significantly. Coinjection of MO with case-specific variant mRNA (encoding p.Gly20Arg and p.Ile83Met) resulted in significantly reduced ability to rescue CH and body length compared with *SIN3B* WT mRNA ($n = 41-61$ larvae/batch, repeated). p.Pro767Leu is a negative control variant (rs117307745; six homozygotes in gnomAD). Statistical analyses were performed via a non-parametric Kruskal-Wallis test. **** $p < 0.0001$; *** $p < 0.001$; ** $p < 0.01$; * $p < 0.05$; ns, not significant; error bars represent standard error of the mean.

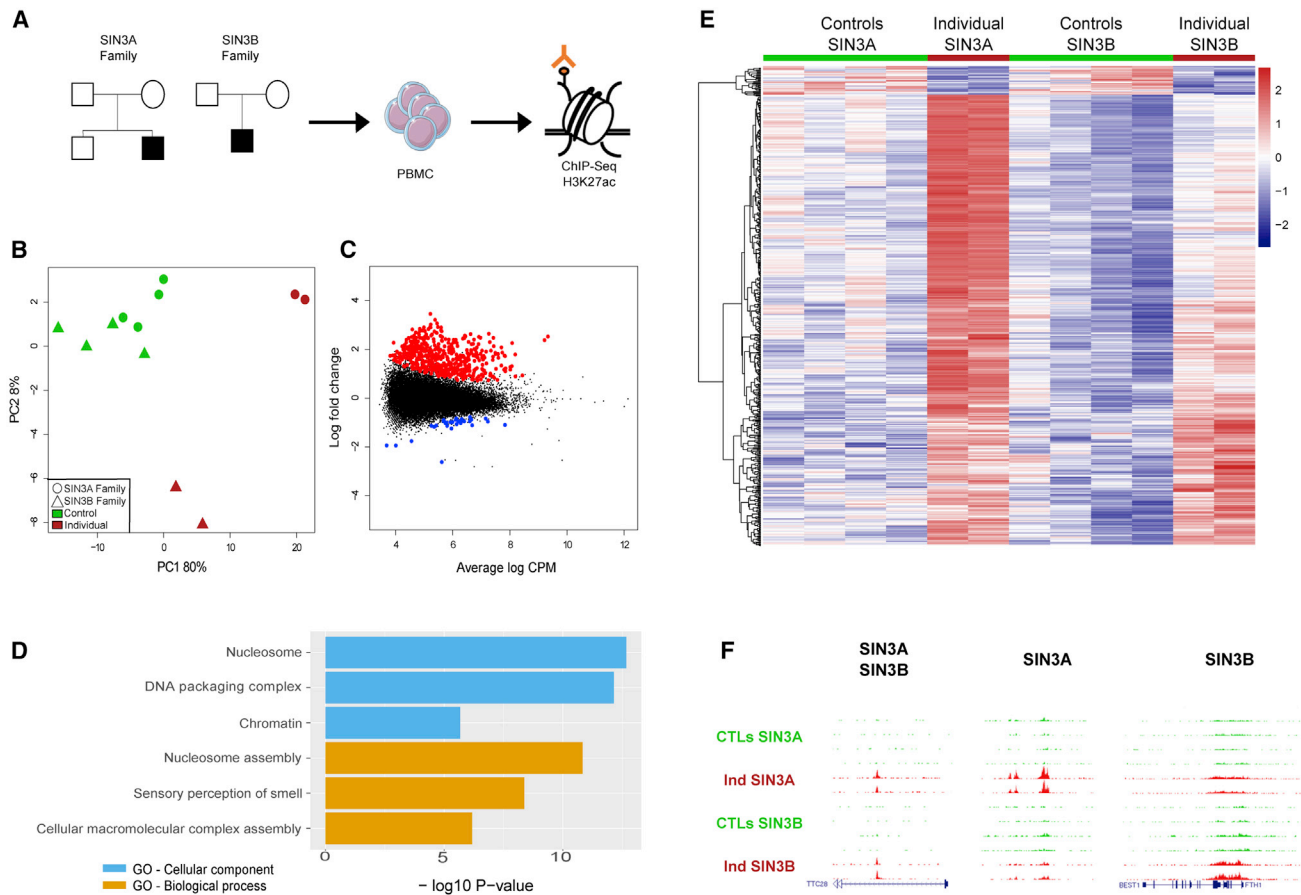


Figure 5. Histone acetylation (H3K27ac) analysis in cells derived from affected individuals with *SIN3A* or *SIN3B* deletion CNVs compared with within-pedigree control individuals reveals hyperacetylation in affected individuals

(A) Diagram showing the experimental approach of the ChIP-seq H3K27ac analysis performed on peripheral blood mononuclear cells (PBMCs) from affected individuals compared with their healthy family members. We characterized genome-wide histone acetylation changes in one individual with a *SIN3A* deletion (individual 4 in Witteveen et al.¹⁵ with a ~350 kb microdeletion) and individual 1 from this study with a *SIN3B* deletion (see Figure 1).

(B) PCA (principal-component analysis) plot of peak heights from the 532 differentially acetylated peaks between all control individuals compared with affected individuals.

(C) MA (log ratio-mean average) plot showing hyperacetylated (red) and hypoacetylated (blue) peaks for both *SIN3A/B*-affected individuals versus all control individuals.

(D) Top three most significant functional groups corresponding to hyperacetylated peaks. GO, gene ontology.

(E) Heatmap of unsupervised clustering of differentially acetylated peaks; Z scores were calculated from normalized counts per million reads.

(F) Representative ChIP-seq genome browser tracks highlighting commonly hyperacetylated peaks in *SIN3A* and *SIN3B* deletion-bearing individuals (left) and exemplar hyperacetylated peaks distinct to either *SIN3A* (center)- or *SIN3B* (right)-affected individuals. CTL, control; Ind, affected individual.

pathogenicity of the p.Gly20Arg and p.Ile83Met variants, we compared the efficiency of variant *SIN3B* mRNA to rescue the morphant phenotype versus WT mRNA for both craniofacial patterning and body length. We used a common variant from gnomAD, p.Pro767Leu, as a negative control (dbSNP: rs117307745, six homozygotes in 282,500 individuals). In replicate experiments, the case-associated SNVs scored as hypomorphic (significantly less rescue than WT mRNA but also different from MO alone). However, the negative control variant scored consistently as benign (not significantly different from WT mRNA rescue; Figure 4F). Finally, to rule out a gain-of-function hypothesis for the nonsynonymous variants and exclude an effect of WT mRNA alone on the detected phenotypes, we

confirmed that expression of WT or case-associated variant human *SIN3B* mRNA does not induce craniofacial defects or body length variations in injected larvae at 3 dpf ($n = 36\text{--}46$ larvae/batch; repeated; Figures S4A and S4B). Together, our *in vivo* complementation data in larval zebrafish with mutation or suppression of *sin3b* reinforce the deleterious effects of *SIN3B* haploinsufficiency resulting in the clinical features noted in our human cohort.

To investigate the consequences of *SIN3B* alteration on gene regulation, we used histone H3 K27 acetylation (H3K27ac) ChIP-seq to map genome-wide enhancer and promoter states in cells derived from an individual carrying a *de novo* *SIN3B* deletion and his healthy family members (individual 1; Figure 5A). H3K27ac is a histone mark found

at active gene regulatory elements (enhancers and promoters) and is thought to be highly cell type specific.^{37,38} This mark is therefore used to define active gene regulatory elements, and because of its robustness, this mark has been used to identify disease-specific mechanisms, especially for neurodevelopmental and degenerative disorders.^{39,40} Here, we used the genome-wide distribution of this mark to test whether the regulatory landscape is altered in PBMCs, which would suggest that the putative repressor gene function of *SIN3B* is abrogated. Because *SIN3A* is thought to have a similar molecular function,⁴¹ we also profiled an individual with a *SIN3A* deletion (individual 4 from Witteveen et al.¹⁵ with a ~350 kb microdeletion) to test whether *SIN3A* and *SIN3B* gene disruption leads to similar epigenetic alterations. For comparison with healthy individuals, we also profiled PBMCs from the healthy parents of the *SIN3A* and *SIN3B* deletion-bearing individuals as well as the unaffected brother of the individual with the *SIN3A* (Figure 5A).

For each individual, we isolated PBMCs and performed two replicate H3K27ac ChIP-seq experiments. We sequenced ChIP-seq libraries and performed quality control analysis; two samples were removed because of a low fraction of reads in peaks (FrIP) or low non-redundant fraction (NRF) (see supplemental methods and Table S5). For each of the remaining samples, we called peaks by using dfilter⁴² (average N of peaks = 23,043), merged all the peaks, and counted reads for each sample within the merged peak set. We used these peaks to calculate differential acetylation peaks between the individuals with *SIN3A* and *SIN3B* CNVs and their within-pedigree control individuals. In total, we found 500 upregulated and 32 downregulated peaks at an FDR cut-off of 5%. Principal-component analysis (PCA) of differential peaks reveals that while the healthy control individuals cluster together, the profiles from *SIN3A* and *SIN3B* CNV carriers are distinct, suggesting that their epigenomic state is altered (Figure 5B). Notably, more peaks were upregulated than downregulated, suggesting that *SIN3A* and *SIN3B* contribute to repressor function of enhancers and promoters in PBMCs (Figure 5C). To categorize the biological functions of genes with altered H3K27ac profiles, we performed Gene Ontology analysis. Among the gene regulatory elements upregulated in either mutant context, we found that various gene pathways are altered, and nucleosome assembly was the most significantly enriched (Figure 5D).

To investigate potential differences in regulatory elements influenced by either *SIN3A* or *SIN3B* independently, we analyzed differential peaks identified in each sample. These were detected when each individual was compared with his respective family members (Figure S5A), suggesting that haploinsufficiency of either *SIN3A* or *SIN3B* leads to hyperacetylation at several loci. Importantly, the epigenetic alterations observed in affected individuals with *SIN3A* and *SIN3B* CNVs were distinct in their intensity, suggesting that although they may be part of the same complex, their regulatory function appears to be non-redundant

(Figure 5E). For example, analysis of specific loci shows that some peaks are altered similarly (e.g., *TTC28* [MIM: 615098]), while other peaks are *SIN3A* or *SIN3B* specific (Figure 5F). Overall, fold changes between affected individuals and control individuals were similar for 16% of hyperacetylated peaks ($\log_{2}FC > 1.5$; Figure S5B). These data are supported further by the observation that peaks significantly upregulated in the context of *SIN3A* haploinsufficiency are also significantly upregulated in the *SIN3B* mutant cells as compared with in-family controls ($p < 0.001$); there was a similar observation in the reciprocal context (peaks significantly upregulated in *SIN3B* mutant cells are also significantly upregulated in *SIN3A* CNV-bearing cells [$p < 0.001$]; Figure S5C). Taken together, these results suggest that, as is the case for heterozygous deletion of *SIN3A*, heterozygous *SIN3B* deletion leads to epigenetic alterations at specific loci in circulating immune cells, a cell type shown previously as a reasonable proxy for neurodevelopmental traits.⁴³ However, we are cautious in the interpretation of our data and recognize the need to analyze cells from additional *SIN3A* and *SIN3B* pedigrees, particularly those with single-gene deletions or pathogenic SNVs.

Here, we show genetic and *in vivo* modeling evidence that *de novo* *SIN3B* pathogenic variants cause a neurodevelopmental syndrome characterized by syndromic ID/DD with variable ASD, growth defects, congenital anomalies, and dysmorphic craniofacial features. Variants in epigenetic regulators, and particularly in genes modulating histone acetylation, have been associated previously with several neurodevelopmental disorders, reinforcing the importance for tightly regulated histone post-translational modification events. For example, disruptive variants in *HDAC4* (MIM: 605314) likely resulting in haploinsufficiency have been described in individuals with brachydactyly-mental retardation syndrome^{44,45} (MIM: 600430). Additionally, *HDAC8* (MIM: 300269) loss-of-function variants cause an X-linked form of Cornelia de Lange syndrome^{46,47} (MIM: 300882), although the likely pathogenic mechanism is impairment of cohesin subunit SMC3 deacetylation by HDAC8. These rare disorders exemplify how histone deacetylation acts as a key molecular process during human development. Moreover, although no Mendelian disorder has been associated with disrupted *HDAC7* (MIM: 606542) in humans, *Hdac7*^{-/-} mice are embryonic lethal.⁴⁸ *Hdac1* and *Hdac2* disruption in mice leads to developmental defects.⁴⁸ Homozygous mouse *Sin3b* mutants display embryonic development defects at embryonic day (E) 13.5 with increased mortality rate and a growth retardation phenotype.⁴⁹

The closely related *SIN3A* paralog (48% similarity to *SIN3B* protein sequence, CLUSTALW v.1.81, multiple sequence alignment, GenBank: NP_056075; Figure S6), located on chromosome 15q24.2, has been associated with syndromic ID and ASD.¹⁵ Clinical features of *SIN3A*-affected individuals include mild ID, recognizable facial gestalt, abnormalities in brain MRIs including ventricular dilatation, corpus callosum dysgenesis, and aberrant

cortical development. Some affected individuals were also described with ASD, seizures, microcephaly, and short stature. *In vivo* knockdown of *Sin3a* in mice impairs cortical neurogenesis, leading to a decreased number of cortical progenitors and altered cortical projections in the developing brain. Clinical features described in our *SIN3B* cohort overlap with previously described phenotypes associated with the *SIN3A*-related disorder. Our H3K27ac ChIP-seq experiments on cells from *SIN3A* and *SIN3B* CNV deletion pedigrees offer initial molecular insight to explain these similarities as well as subtle differences.

In summary, our data expand the phenotypic spectrum associated with *Sin3* complex haploinsufficiency to syndromic ID/ASD, arguing against the functional redundancy of *SIN3A* and *SIN3B*. Our findings confirm the importance of *Sin3* complex integrity for central nervous system development, anterior cartilage patterning, and growth and highlight a major role for *SIN3B* in this process.

Data and code availability

The NCBI reference sequence numbers for human *SIN3B* transcript and zebrafish *sin3b* transcript are GenBank NM_015260.4 and NP_056075.1 (hg19) and GenBank: NM_001044945 and NP_001038410 (GRCz10), respectively.

Supplemental information

Supplemental information can be found online at <https://doi.org/10.1016/j.ajhg.2021.03.017>.

Acknowledgments

We are grateful to individuals who participated in the study. We also thank Mr. Z. Kupchinsky and Mr. I. Pediaditakis for zebrafish husbandry; Mr. D. Morrow for assisting with reagents for *in vivo* modeling studies; and members of the Center for Human Disease Modeling for helpful discussions. This work was supported by funds from US NIH grant R01 HD096326 to N.K. and R01 MH106826 to E.E.D.

Declaration of interests

S.S. and K.M. are employees of GeneDx, Inc., a wholly owned subsidiary of OPKO Health, Inc. N.K. is a paid consultant for and holds significant stock of Rescindo Therapeutics, Inc. The Department of Molecular and Human Genetics at Baylor College of Medicine derives revenue from clinical genetic testing conducted at Baylor Genetics Laboratory.

Received: September 23, 2019

Accepted: March 18, 2021

Published: April 2, 2021

Web resources

1000 Genomes, <https://www.internationalgenome.org/>
CHOPCHOP, <http://chopchop.cbu.uib.no/>
ClinVar, <https://www.ncbi.nlm.nih.gov/clinvar/>

Database of Genomic Variants (DGV), <http://dgv.tcag.ca/dgv/app/home>

dbSNP, <https://www.ncbi.nlm.nih.gov/projects/SNP/>

DECIPHER, <https://decipher.sanger.ac.uk/>

ExAC browser, <http://exac.broadinstitute.org/>

Exome Variant Server, <https://evs.gs.washington.edu/EVS/>

GenBank, <https://www.ncbi.nlm.nih.gov/genbank/>

GeneMatcher, <https://genematcher.org/>

gnomAD browser, <https://gnomad.broadinstitute.org/>

OMIM, <https://omim.org/>

Primer3, <https://bioinfo.ut.ee/primer3>

SMART, <http://smart.emblheidelberg.de/smart/>

References

1. Izumi, K. (2016). Disorders of Transcriptional Regulation: An Emerging Category of Multiple Malformation Syndromes. *Mol. Syndromol.* 7, 262–273.
2. Tebbenkamp, A.T.N., Willsey, A.J., State, M.W., and Sestan, N. (2014). The developmental transcriptome of the human brain: implications for neurodevelopmental disorders. *Curr. Opin. Neurol.* 27, 149–156.
3. Chen, L.-F., Zhou, A.S., and West, A.E. (2017). Transcribing the connectome: roles for transcription factors and chromatin regulators in activity-dependent synapse development. *J. Neurophysiol.* 118, 755–770.
4. Larizza, L., and Finelli, P. (2019). Developmental disorders with intellectual disability driven by chromatin dysregulation: Clinical overlaps and molecular mechanisms. *Clin. Genet.* 95, 231–240.
5. Lopez-Atalaya, J.P., Valor, L.M., and Barco, A. (2014). Epigenetic factors in intellectual disability: the Rubinstein-Taybi syndrome as a paradigm of neurodevelopmental disorder with epigenetic origin. *Prog. Mol. Biol. Transl. Sci.* 128, 139–176.
6. Bjornsson, H.T. (2015). The Mendelian disorders of the epigenetic machinery. *Genome Res.* 25, 1473–1481.
7. Nan, X., Ng, H.H., Johnson, C.A., Laherty, C.D., Turner, B.M., Eisenman, R.N., and Bird, A. (1998). Transcriptional repression by the methyl-CpG-binding protein MeCP2 involves a histone deacetylase complex. *Nature* 393, 386–389.
8. Zhang, Y., Iratni, R., Erdjument-Bromage, H., Tempst, P., and Reinberg, D. (1997). Histone deacetylases and SAP18, a novel polypeptide, are components of a human Sin3 complex. *Cell* 89, 357–364.
9. Knoepfler, P.S., and Eisenman, R.N. (1999). Sin meets NuRD and other tails of repression. *Cell* 99, 447–450.
10. Grimes, J.A., Nielsen, S.J., Battaglioli, E., Miska, E.A., Speh, J.C., Berry, D.L., Atouf, F., Holdener, B.C., Mandel, G., and Kouzarides, T. (2000). The co-repressor mSin3A is a functional component of the REST-CoREST repressor complex. *J. Biol. Chem.* 275, 9461–9467.
11. Kadamb, R., Mittal, S., Bansal, N., Batra, H., and Saluja, D. (2013). Sin3: insight into its transcription regulatory functions. *Eur. J. Cell Biol.* 92, 237–246.
12. van Oevelen, C., Wang, J., Asp, P., Yan, Q., Kaelin, W.G., Jr., Kluger, Y., and Dynlacht, B.D. (2008). A role for mammalian Sin3 in permanent gene silencing. *Mol. Cell* 32, 359–370.
13. Alland, L., David, G., Shen-Li, H., Potes, J., Muhle, R., Lee, H.-C., Hou, H., Jr., Chen, K., and DePinho, R.A. (2002). Identification of mammalian Sds3 as an integral component of the

- Sin3/histone deacetylase corepressor complex. *Mol. Cell. Biol.* 22, 2743–2750.
14. Laherty, C.D., Yang, W.M., Sun, J.M., Davie, J.R., Seto, E., and Eisenman, R.N. (1997). Histone deacetylases associated with the mSin3 corepressor mediate mad transcriptional repression. *Cell* 89, 349–356.
 15. Witteveen, J.S., Willemsen, M.H., Dombroski, T.C.D., van Bakel, N.H.M., Nillesen, W.M., van Hulten, J.A., Jansen, E.J.R., Verkaik, D., Veenstra-Knol, H.E., van Ravenswaaij-Arts, C.M.A., et al. (2016). Haploinsufficiency of MeCP2-interacting transcriptional co-repressor SIN3A causes mild intellectual disability by affecting the development of cortical integrity. *Nat. Genet.* 48, 877–887.
 16. Aten, E., den Hollander, N., Ruivenkamp, C., Knijnenburg, J., van Bokhoven, H., den Dunnen, J., and Breuning, M. (2009). Split hand-foot malformation, tetralogy of Fallot, mental retardation and a 1 Mb 19p deletion-evidence for further heterogeneity? *Am. J. Med. Genet. A.* 149A, 975–981.
 17. Bens, S., Haake, A., Tönnies, H., Vater, I., Stephani, U., Holterhus, P.-M., Siebert, R., and Caliebe, A. (2011). A de novo 1.1Mb microdeletion of chromosome 19p13.11 provides indirect evidence for EPS15L1 to be a strong candidate for split hand split foot malformation. *Eur. J. Med. Genet.* 54, e501–e504.
 18. Lek, M., Karczewski, K.J., Minikel, E.V., Samocha, K.E., Banks, E., Fennell, T., O'Donnell-Luria, A.H., Ware, J.S., Hill, A.J., Cummings, B.B., et al.; Exome Aggregation Consortium (2016). Analysis of protein-coding genetic variation in 60,706 humans. *Nature* 536, 285–291.
 19. Gripp, K.W., Wotton, D., Edwards, M.C., Roessler, E., Ades, L., Meinecke, P., Richieri-Costa, A., Zackai, E.H., Massagué, J., Muenke, M., and Elledge, S.J. (2000). Mutations in TGIF cause holoprosencephaly and link NODAL signalling to human neural axis determination. *Nat. Genet.* 25, 205–208.
 20. Cheong, S.-S., Hentschel, L., Davidson, A.E., Gerrelli, D., Davie, R., Rizzo, R., Pontikos, N., Plagnol, V., Moore, A.T., Sowden, J.C., et al. (2016). Mutations in CPAMD8 Cause a Unique Form of Autosomal-Recessive Anterior Segment Dysgenesis. *Am. J. Hum. Genet.* 99, 1338–1352.
 21. Martínez, F., Caro-Llopis, A., Roselló, M., Oltra, S., Mayo, S., Monfort, S., and Orellana, C. (2017). High diagnostic yield of syndromic intellectual disability by targeted next-generation sequencing. *J. Med. Genet.* 54, 87–92.
 22. Sobreira, N., Schiettecatte, F., Valle, D., and Hamosh, A. (2015). GeneMatcher: a matching tool for connecting investigators with an interest in the same gene. *Hum. Mutat.* 36, 928–930.
 23. De Franco, E., Watson, R.A., Weninger, W.J., Wong, C.C., Flanagan, S.E., Caswell, R., Green, A., Tudor, C., Lelliott, C.J., Geyer, S.H., et al. (2019). A Specific CNOT1 Mutation Results in a Novel Syndrome of Pancreatic Agenesis and Holoprosencephaly through Impaired Pancreatic and Neurological Development. *Am. J. Hum. Genet.* 104, 985–989.
 24. Kruszka, P., Berger, S.I., Weiss, K., Everson, J.L., Martinez, A.F., Hong, S., Anyane-Yeboah, K., Lipinski, R.J., and Muenke, M. (2019). A CCR4-NOT Transcription Complex, Subunit 1, CNOT1, Variant Associated with Holoprosencephaly. *Am. J. Hum. Genet.* 104, 990–993.
 25. Vissers, L.E.L.M., Kalvakuri, S., de Boer, E., Geuer, S., Oud, M., van Outersterp, I., Kwint, M., Witmond, M., Kersten, S., Polla, D.L., et al.; DDD Study (2020). De Novo Variants in CNOT1, a Central Component of the CCR4-NOT Complex Involved in Gene Expression and RNA and Protein Stability, Cause Neurodevelopmental Delay. *Am. J. Hum. Genet.* 107, 164–172.
 26. Moravec, C.E., Yousef, H., Kinney, B.A., Salerno-Eichenholz, R., Monestime, C.M., Martin, B.L., and Sirotkin, H.I. (2017). Zebrafish *sin3b* mutants are viable but have size, skeletal, and locomotor defects. *Dev. Dyn.* 246, 946–955.
 27. Shaw, N.D., Brand, H., Kupchinsky, Z.A., Bengani, H., Plummer, L., Jones, T.I., Erdin, S., Williamson, K.A., Rainger, J., Stortchevoi, A., et al. (2017). SMCHD1 mutations associated with a rare muscular dystrophy can also cause isolated arhinia and Bosma arhinia microphthalmia syndrome. *Nat. Genet.* 49, 238–248.
 28. Rooryck, C., Diaz-Font, A., Osborn, D.P.S., Chabchoub, E., Hernandez-Hernandez, V., Shamseldin, H., Kenny, J., Waters, A., Jenkins, D., Kaissi, A.A., et al. (2011). Mutations in lectin complement pathway genes COLEC11 and MASP1 cause 3MC syndrome. *Nat. Genet.* 43, 197–203.
 29. Beunders, G., Voorhoeve, E., Golzio, C., Pardo, L.M., Rosenfeld, J.A., Talkowski, M.E., Simonic, I., Lionel, A.C., Vergult, S., Pyatt, R.E., et al. (2013). Exonic deletions in *AUTS2* cause a syndromic form of intellectual disability and suggest a critical role for the C terminus. *Am. J. Hum. Genet.* 92, 210–220.
 30. Stankiewicz, P., Khan, T.N., Szafranski, P., Slattery, L., Streff, H., Vetrini, F., Bernstein, J.A., Brown, C.W., Rosenfeld, J.A., Rednam, S., et al.; Deciphering Developmental Disorders Study (2017). Haploinsufficiency of the Chromatin Remodeler BPTF Causes Syndromic Developmental and Speech Delay, Postnatal Microcephaly, and Dysmorphic Features. *Am. J. Hum. Genet.* 101, 503–515.
 31. Küry, S., Besnard, T., Ebstein, F., Khan, T.N., Gambin, T., Douglas, J., Bacino, C.A., Craigen, W.J., Sanders, S.J., Lehmann, A., et al. (2017). De Novo Disruption of the Proteasome Regulatory Subunit PSMD12 Causes a Syndromic Neurodevelopmental Disorder. *Am. J. Hum. Genet.* 100, 352–363.
 32. Frosk, P., Arts, H.H., Philippe, J., Gunn, C.S., Brown, E.L., Chodirker, B., Simard, L., Majewski, J., Fahiminiya, S., Russell, C., et al.; FORGE Canada Consortium; and Canadian Rare Diseases: Models & Mechanisms Network (2017). A truncating mutation in *CEP55* is the likely cause of MARCH, a novel syndrome affecting neuronal mitosis. *J. Med. Genet.* 54, 490–501.
 33. Isrie, M., Breuss, M., Tian, G., Hansen, A.H., Cristofoli, F., Morandell, J., Kupchinsky, Z.A., Sifrim, A., Rodriguez-Rodriguez, C.M., Dapena, E.P., et al. (2015). Mutations in Either *TUBB* or *MAPRE2* Cause Circumferential Skin Creases Kunze Type. *Am. J. Hum. Genet.* 97, 790–800.
 34. Kague, E., Gallagher, M., Burke, S., Parsons, M., Franz-Odenaal, T., and Fisher, S. (2012). Skeletogenic fate of zebrafish cranial and trunk neural crest. *PLoS ONE* 7, e47394.
 35. Ansar, M., Ullah, F., Paracha, S.A., Adams, D.J., Lai, A., Pais, L., Iwaszkiewicz, J., Millan, F., Sarwar, M.T., Agha, Z., et al. (2019). Bi-allelic Variants in *DYNC112* Cause Syndromic Microcephaly with Intellectual Disability, Cerebral Malformations, and Dysmorphic Facial Features. *Am. J. Hum. Genet.* 104, 1073–1087.
 36. Niederriter, A.R., Davis, E.E., Golzio, C., Oh, E.C., Tsai, I.-C., and Katsanis, N. (2013). In vivo modeling of the morbid human genome using *Danio rerio*. *J. Vis. Exp.* 78, e50338.
 37. ENCODE Project Consortium (2012). An integrated encyclopedia of DNA elements in the human genome. *Nature* 489, 57–74.
 38. Kundaje, A., Meuleman, W., Ernst, J., Bilenyk, M., Yen, A., Heravi-Moussavi, A., Kheradpour, P., Zhang, Z., Wang, J., Ziller,

- M.J., et al.; Roadmap Epigenomics Consortium (2015). Integrative analysis of 111 reference human epigenomes. *Nature* 518, 317–330.
39. Marzi, S.J., Leung, S.K., Ribarska, T., Hannon, E., Smith, A.R., Pishva, E., Poschmann, J., Moore, K., Troakes, C., Al-Sarraj, S., et al. (2018). A histone acetylome-wide association study of Alzheimer's disease identifies disease-associated H3K27ac differences in the entorhinal cortex. *Nat. Neurosci.* 21, 1618–1627.
 40. Sun, W., Poschmann, J., Cruz-Herrera Del Rosario, R., Parikshak, N.N., Hajan, H.S., Kumar, V., Ramasamy, R., Belgard, T.G., Elanggovan, B., Wong, C.C.Y., et al. (2016). Histone Acetylome-wide Association Study of Autism Spectrum Disorder. *Cell* 167, 1385–1397.e11.
 41. Bainor, A.J., Saini, S., Calderon, A., Casado-Polanco, R., Giner-Ramirez, B., Moncada, C., Cantor, D.J., Ernlund, A., Litovchick, L., and David, G. (2018). The HDAC-Associated Sin3B Protein Represses DREAM Complex Targets and Cooperates with APC/C to Promote Quiescence. *Cell Rep.* 25, 2797–2807.e8.
 42. Kumar, V., Muratani, M., Rayan, N.A., Kraus, P., Lufkin, T., Ng, H.H., and Prabhakar, S. (2013). Uniform, optimal signal processing of mapped deep-sequencing data. *Nat. Biotechnol.* 31, 615–622.
 43. Migliavacca, E., Golzio, C., Männik, K., Blumenthal, I., Oh, E.C., Harewood, L., Kosmicki, J.A., Loviglio, M.N., Giannuzzi, G., Hippolyte, L., et al.; 16p11.2 European Consortium (2015). A Potential Contributory Role for Ciliary Dysfunction in the 16p11.2 600 kb BP4-BP5 Pathology. *Am. J. Hum. Genet.* 96, 784–796.
 44. Villavicencio-Lorini, P., Klopocki, E., Trimborn, M., Koll, R., Mundlos, S., and Horn, D. (2013). Phenotypic variant of Brachydactyly-mental retardation syndrome in a family with an inherited interstitial 2q37.3 microdeletion including HDAC4. *Eur. J. Hum. Genet.* 21, 743–748.
 45. Wheeler, P.G., Huang, D., and Dai, Z. (2014). Haploinsufficiency of HDAC4 does not cause intellectual disability in all affected individuals. *Am. J. Med. Genet. A.* 164A, 1826–1829.
 46. Harakalova, M., van den Boogaard, M.-J., Sinke, R., van Lieshout, S., van Tuil, M.C., Duran, K., Renkens, I., Terhal, P.A., de Kovel, C., Nijman, I.J., et al. (2012). X-exome sequencing identifies a HDAC8 variant in a large pedigree with X-linked intellectual disability, truncal obesity, gynecomastia, hypogonadism and unusual face. *J. Med. Genet.* 49, 539–543.
 47. Deardorff, M.A., Bando, M., Nakato, R., Watrin, E., Itoh, T., Minamino, M., Saitoh, K., Komata, M., Katou, Y., Clark, D., et al. (2012). HDAC8 mutations in Cornelia de Lange syndrome affect the cohesin acetylation cycle. *Nature* 489, 313–317.
 48. Montgomery, R.L., Hsieh, J., Barbosa, A.C., Richardson, J.A., and Olson, E.N. (2009). Histone deacetylases 1 and 2 control the progression of neural precursors to neurons during brain development. *Proc. Natl. Acad. Sci. USA* 106, 7876–7881.
 49. David, G., Grandinetti, K.B., Finnerty, P.M., Simpson, N., Chu, G.C., and Depinho, R.A. (2008). Specific requirement of the chromatin modifier mSin3B in cell cycle exit and cellular differentiation. *Proc. Natl. Acad. Sci. USA* 105, 4168–4172.